Rheological properties of binary and ternary amphiphilic fluid mixtures

Rheological Properties of Binary and Ternary Amphiphilic Fluid Mixtures

Jens Harting[1] and Giovanni Giupponi[2]

[1] Institut für Computerphysik, Pfaffenwaldring 27, 70569 Stuttgart, Germany
[2] Centre for Computational Science, Chemistry Department,
University College London, 20 Gordon Street, London WC1H 0AJ, UK

Abstract. Within this project, we perform lattice Boltzmann simulations of spinodal decomposition and structuring effects in binary immiscible and ternary amphiphilic fluid mixtures under shear. We use a highly scalable parallel Fortran 90 code for the implementation of the lattice Boltzmann method. We demonstrate that the domain growth mechanisms in ternary amphiphilic fluid mixtures strongly depend on the amphiphile concentration. For systems under constant and oscillatory shear we analyze domain growth rates in directions parallel and perpendicular to the applied shear and find that these systems undergo structural transitions with tubular and lamellar structures appearing.

1 Introduction

In recent years there has emerged a class of fluid dynamical problems, called "complex fluids", which involve both hydrodynamic flow effects and complex interactions between fluid particles. Computationally, such problems are too large and expensive to tackle with atomistic methods such as molecular dynamics, yet they require too much molecular detail for continuum Navier–Stokes approaches.

Algorithms which work at an intermediate or "mesoscale" level of description in order to solve these problems have been developed within the last two decades. These include Dissipative Particle Dynamics [5, 14, 7], Lattice Gas Cellular Automata [19], Stochastic Rotation Dynamics [17, 11, 20], and the Lattice Boltzmann method [23, 1, 16]. In particular, the Lattice Boltzmann method has been found highly useful for the simulation of complex fluid flows in a wide variety of systems. This algorithm is extremely well suited to be implemented on parallel computers, which permits very large systems to be simulated, reaching hitherto inaccessible physical regimes.

"Simple fluids" usually can be described to a good degree of approximation by macroscopic quantities only, such as the density $\rho(\mathbf{x})$, velocity $\mathbf{v}(\mathbf{x})$, and temperature $T(\mathbf{x})$. Such fluids are governed by the Navier–Stokes Eq. [6],

which are nonlinear and difficult to solve in the most general case, with the result that numerical solution of the equations has become a common tool for understanding the behaviour of "simple" fluids, such as water or air. "Complex fluids" on the other hand are fluids where the macroscopic flow is affected by microscopic properties. A good example of such a fluid is blood: as it flows through vessels, it is subjected to shear forces, which cause red blood cells to align with the flow so that they can slide over one another more easily. This effect causes a change in viscosity which in turn affects the flow profile. Hence, the macroscopic blood flow is affected by the microscopic alignment of its constituent cells. Other examples of complex fluids include fluids such as paint, milk, cell organelles, as well as polymers and liquid crystals. In all of these cases, the density and velocity fields are insufficient to describe the fluid behaviour, and in order to understand this behaviour, it is necessary to treat effects which occur over a very wide range of length and time scales. This length and time scale gap makes complex fluids even more difficult to model.

In a mixture containing various fluid components, an amphiphile is a molecule which is composed of two parts, each part being attracted towards a different fluid component. For example, soap molecules are amphiphiles, containing a head group which is attracted towards water, and a tail which is attracted towards oil. If many amphiphile molecules are collected together in solution, they can exhibit highly varied and complicated behaviour, often assembling to form amphiphile mesophases, which are complex fluids of significant theoretical and industrial importance. Some of these phases have long-range order, yet remain able to flow, and are called liquid crystal mesophases.

Within this project we have performed large scale lattice-Boltzmann simulations in order to study the bahaviour of binary immiscible or ternary amphiphilic fluid mixtures under shear. Since in our case the amphiphilic molecules can be seen as surfactant, we will also use the latter term in this paper.

1.1 The Model

A standard LB system involving multiple species is usually represented by a set of equations [13]

$$n_i^\alpha(\mathbf{x}+\mathbf{c}_i, t+1) - n_i^\alpha(\mathbf{x}, t) = -\tfrac{1}{\tau_\alpha}(n_i^\alpha(\mathbf{x}, t) - n_i^{\alpha eq}(\mathbf{x}, t)),\ i = 0, 1, \ldots, b\ , \tag{1}$$

where $n_i^\alpha(\mathbf{x}, t)$ is the single-particle distribution function, indicating the density of species α (for example, oil, water or amphiphile), having velocity $\mathbf{c}_i$, at site $\mathbf{x}$ on a D-dimensional lattice of coordination number b, at time-step t. The collision operator Ω_i^α represents the change in the single-particle distribution function due to the collisions. We choose a single relaxation time τ_α, 'BGK' form [2] for the collision operator. In the limit of low Mach numbers, the LB equations correspond to a solution of the Navier-Stokes equation

for isothermal, quasi-incompressible fluid flow whose implementation can efficiently exploit parallel computers, as the dynamics at a point requires only information about quantities at nearest neighbour lattice sites. The local equilibrium distribution $n_i^{\alpha eq}$ plays a fundamental role in the dynamics of the system as shown by Eq. (1). In this study, we use a purely kinetic approach, for which the local equilibrium distribution $n_i^{\alpha eq}(\mathbf{x}, t)$ is derived by imposing certain restrictions on the microscopic processes, such as explicit mass and total momentum conservation [4]

$$n_i^{\alpha eq} = \zeta_i n^\alpha \left[1 + \frac{\mathbf{c}_i \cdot \mathbf{u}}{c_s^2} + \frac{(\mathbf{c}_i \cdot \mathbf{u})^2}{2c_s^4} - \frac{u^2}{2c_s^2} + \frac{(\mathbf{c}_i \cdot \mathbf{u})^3}{6c_s^6} - \frac{u^2(\mathbf{c}_i \cdot \mathbf{u})}{2c_s^4}\right] , \quad (2)$$

where $\mathbf{u} = \mathbf{u}(\mathbf{x}, t)$ is the macroscopic bulk velocity of the fluid, defined as $n^\alpha(\mathbf{x}, t)\mathbf{u}^\alpha \equiv \sum_i n_i^\alpha(\mathbf{x}, t)\mathbf{c}_i$, ζ_i are the coefficients resulting from the velocity space discretization and c_s is the speed of sound, both of which are determined by the choice of the lattice, which is D3Q19 in our implementation. Immiscibility of species α is introduced in the model following Shan and Chen [21, 22]. Only nearest neighbour interactions among the immiscible species are considered. These interactions are modelled as a self-consistently generated mean field body force

$$\mathbf{F}^\alpha(\mathbf{x}, t) \equiv -\psi^\alpha(\mathbf{x}, t) \sum_{\bar{\alpha}} g_{\alpha\bar{\alpha}} \sum_{\mathbf{x}'} \psi^{\bar{\alpha}}(\mathbf{x}', t)(\mathbf{x}' - \mathbf{x}) , \quad (3)$$

where $\psi^\alpha(\mathbf{x}, t)$ is the so-called effective mass, which can have a general form for modelling various types of fluids (we use $\psi^\alpha = (1 - e^{-n^\alpha})$[21]), and $g_{\bar{\alpha}\alpha}$ is a force coupling constant whose magnitude controls the strength of the interaction between components α, $\bar{\alpha}$ and is set positive to mimic repulsion. The dynamical effect of the force is realized in the BGK collision operator by adding to the velocity $\mathbf{u}$ in the equilibrium distribution of Eq. (2) an increment

$$\delta\mathbf{u}^\alpha = \frac{\tau^\alpha \mathbf{F}^\alpha}{n^\alpha} . \quad (4)$$

As described above, an amphiphile usually possesses two different fragments, each having an affinity for one of the two immiscible components. The addition of an amphiphile is implemented as in [3]. An average dipole vector $\mathbf{d}(\mathbf{x}, t)$ is introduced at each site $\mathbf{x}$ to represent the orientation of any amphiphile present there. The direction of this dipole vector is allowed to vary continuously and no information is specified for each velocity $\mathbf{c}_i$, for reasons of computational efficiency and simplicity. Full details of the model can be found in [3] and [18].

In order to inspect the rheological behaviour of multi-phase fluids, we have implemented Lees-Edwards boundary conditions, which reduce finite size effects if compared to moving solid walls [15]. This computationally convenient method imposes new positions and velocities on particles leaving the simulation box in the direction perpendicular to the imposed shear strain while

leaving the other coordinates unchanged. Choosing z as the direction of shear and x as the direction of the velocity gradient, we have

$$z' \equiv \begin{cases} (z + \Delta_z) \bmod N_z & , x > N_x \\ z \bmod N_z & , 0 \leq x \leq N_x \\ (z - \Delta_z) \bmod N_z & , x < 0 \end{cases} \quad u'_z \equiv \begin{cases} u_z + U & , x > N_x \\ u_z & , 0 \leq x \leq N_x \\ u_z - U & , x < 0 \end{cases} , \quad (5)$$

where $\Delta_z \equiv U\Delta t$, U is the shear velocity, u_z is the $z-$component of $\mathbf{u}$ and $N_{x(z)}$ is the system length in the $x(z)$ direction. We also use an interpolation scheme suggested by Wagner and Pagonabarraga [24] as Δ_z is not generally a multiple of the lattice site. Consistent with the hypothesis of the LB model, we set the maximum shear velocity to $U = 0.1$ lattice units. This results in a maximum shear rate $\dot{\gamma}_{xz} = \frac{2\times 0.1}{64} = 3.2 \times 10^{-3}$ For oscillatory shear, we set

$$U(t) = U \cos(\omega t) \ , \quad (6)$$

where $\omega/2\pi$ is the frequency of oscillation.

2 The Simulation Code

We use LB3D [9], a highly scalable parallel LB code, to implement the model. LB3D is written in Fortran 90 and designed to run on distributed-memory parallel computers, using MPI for communication. In each simulation, the fluid is discretized onto a cubic lattice, each lattice point containing information about the fluid in the corresponding region of space. Each lattice site requires about a kilobyte of memory per lattice site so that, for example, a simulation on a 128^3 lattice would require around 2.2GB memory. The code runs at over $3 \cdot 10^4$ lattice site updates per second per CPU on a recent machine, and has been observed to have roughly linear scaling up to order $3 \cdot 10^3$ compute nodes. Larger simulations have not been possible so far due to the lack of access to a machine with a higer processor count. The largest simulation we performed used a 1024^3 lattice to describe a mesophase consisting of two immiscible and one amphiphilic phase. The output from a simulation usually takes the form of a single floating-point number for each lattice site, representing, for example, the density of a particular fluid component at that site. Therefore, a density field snapshot from a 128^3 system would produce output files of around 8MB. Writing data to disk is one of the bottlenecks in large scale simulations. If one simulates a 1024^3 system, each data file is 4GB in size. LB3D is able to benefit from the parallel filesystems available on many large machines today, by using the MPI-IO based parallel HDF5 data format [12]. Our code is very robust regarding different platforms or cluster interconnects: even with moderate inter-node bandwidths it achieves almost linear scaling for large processor counts with the only limitation being the available memory per node. The platforms our code has been successfully used on include various supercomputers like the NEC SX8, IBM pSeries, SGI Altix and Origin, Cray T3E, Compaq Alpha clusters, as well as low cost 32- and 64-bit Linux clusters.

3 Complex Fluids under Shear

In many industrial applications, complex fluids are subject to shear forces. For example, axial bearings are often filled with fluid to reduce friction and transport heat away from the most vulnerable parts of the device. It is very important to understand how these fluids behave under high shear forces, in order to be able to build reliable machines and choose the proper fluid for different applications. In our simulations we use Lees–Edwards boundary conditions, which were originally developed for molecular dynamics simulations in 1972 [15] and have been used in lattice Boltzmann simulations by different authors before [25, 24, 10]. We apply our model to study the behaviour of binary immiscible and ternary amphiphilic fluids under constant and oscillatory shear. In the non-sheared studies of spinodal decomposition it has been shown that lattice sizes need to be large in order to overcome finite size effects: 128^3 was the minimum acceptable number of lattice sites [8]. For high shear rates, systems also have to be very long because, if the system is too small, the domains interconnect across the $\mathbf{z} = \mathbf{0}$ and $\mathbf{z} = \mathbf{nz}$ boundaries to form interconnected lamellae in the direction of shear. Such artefacts need to be eliminated from our simulations. Figure 1 shows an example from a simulation with lattice size 128x128x512. The volume rendered blue and red areas depict the different fluid species and the arrows denote the direction of shear.

The focus of our current project is on the behaviour of ternary amphiphilic fluids. We are interested in the effect an amphiphilic phase has on the demixing of two immiscible fluids. In all simulations we keep the total density of the system at $\rho^{tot} = \rho^A + \rho^B + \rho^s = 1.6$ and $\rho^A = \rho^B$.

We study a cubic 256^3 system with a total density of 1.6 and surfactant densities $\rho^s = 0.00, 0.10, 0.20, 0.30$. As can be seen in Fig. 2, after 10000 timesteps the phases have separated to a large extend if no surfactant is present. If one adds surfactant, the domains grow more slowly and the growth process might even come to arrest for high amphiphile concentrations.

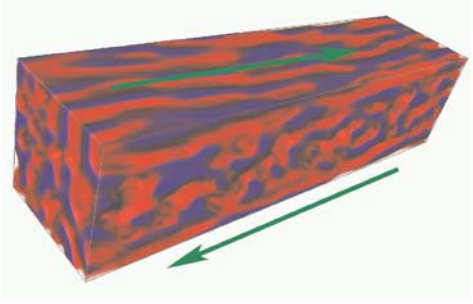

Fig. 1. Spinodal decomposition under shear. *Differently coloured regions* denote the majority of the corresponding fluid. The *arrows* depict the movement of the sheared boundaries

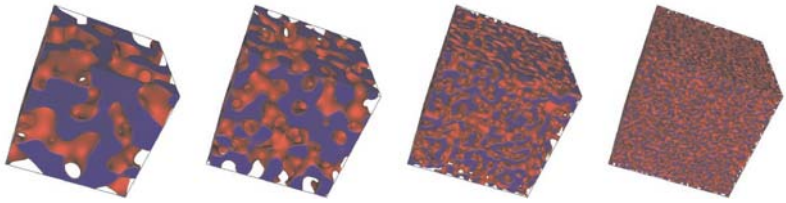

Fig. 2. Volume rendered fluid densities of 256^3 systems at $t = 10000$ for surfactant densities $\rho^s = 0.00,\ 0.10,\ 0.20,\ 0.30$ (*from left to right*)

In order to quantitatively compare between simulations with different surfactant densities, we define the time dependent lateral domain size $L(t)$ along direction $i = x, y, z$ as

$$L_i(t) \equiv \frac{2\pi}{\sqrt{\langle k_i^2(t)\rangle}}, \tag{7}$$

where

$$\left\langle k_i^2(t)\right\rangle \equiv \frac{\sum_{\mathbf{k}} k_i^2 S(\mathbf{k},t)}{\sum_{\mathbf{k}} S(\mathbf{k},t)} \tag{8}$$

is the second order moment of the three-dimensional structure function

$$S(\mathbf{k},t) \equiv \frac{1}{V}\left|\phi'_{\mathbf{k}}(t)\right|^2 \tag{9}$$

with respect to the cartesian component i. $\langle\rangle$ denotes the average in Fourier space, weighted by $S(\mathbf{k})$ and V is the number of nodes of the lattice, $\phi'_{\mathbf{k}}(t)$ the Fourier transform of the fluctuations of the order parameter $\phi' \equiv \phi - \langle\phi\rangle$, and k_i is the ith component of the wave vector.

In Fig. 3 the time dependent lateral domain size $L(t)$ is shown for a number of surfactant densities $\rho^s = 0.00,\ 0.10,\ 0.15,\ 0.20,\ 0.25,\ 0.30,\ 0.35,\ 0.40$, and 0.45. The plots in Fig. 3 confirm what we already expected from the three-dimensional images presented in Fig. 2: For $\rho^s = 0.00$ domain growth dows not come to an end until the domains span the full system. Only by adding surfactant, we can slow down the growth process and for high surfactant densities $\rho^s > 0.25$, the domain growth stops after a few thousand simulation timesteps. By adding even more surfactant, the final average domain size becomes very small. We are currently analysing these results and try to find scaling laws for the dependence of the final domain size and the growth rate on the surfactant density.

Another interesting topic is the influence of shear on the phase separation. Figure 4 shows four examples of systems which are sheared with a constant shear rate $\dot{\gamma} = 1.56 \cdot 10^{-3}$ at $t = 10000$. Again, one observes a decreasing domain size with increasing surfactant concentration. We vary the concentration as $\rho^s = 0.0$ (upper left), 0.1 (upper right), 0.2 (lower left), and 0.3 (lower right). In addition one can also observe structural changes like the formation of lamellae in the system. Lamellae are especially well pronounced for

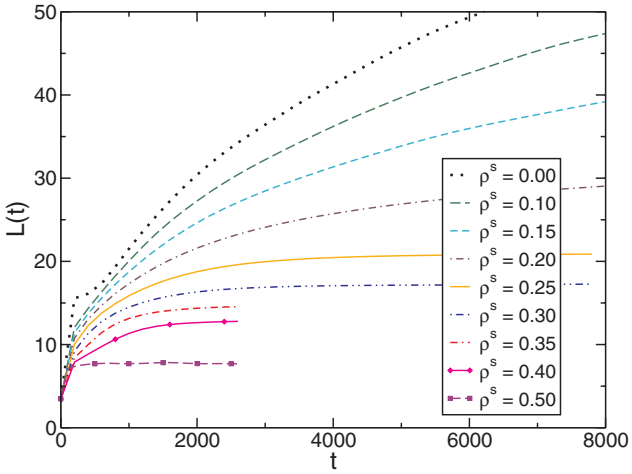

Fig. 3. Average domain size $L(t)$ for various surfactant densities $\rho^s = 0.00$, 0.10, 0.15, 0.20, 0.25, 0.30, 0.35, 0.40, 0.45

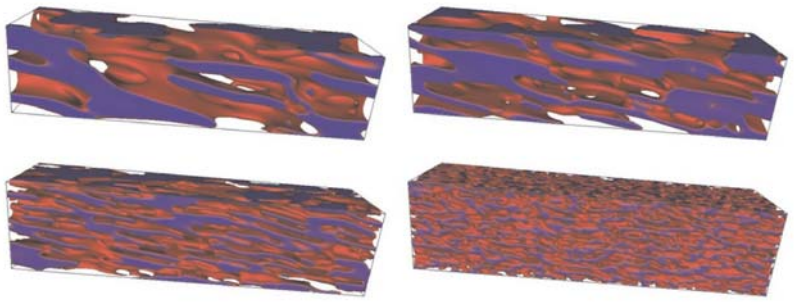

Fig. 4. Volume rendered fluid densities for surfactant densities $\rho^s = 0.0$ (*upper left*), 0.1 (*upper right*), 0.2 (*lower left*), 0.3 (*lower right*), a constant shear rate $\dot{\gamma} = 1.56 \cdot 10^{-3}$ and $t = 10000$

low surfactant concentrations, while for larger concentrations the domains try to form more tube-like structures. The time dependent lateral domain size shows an even richer behaviour as can be seen in Fig. 5. Here, we show the domain size in all three directions, where x denotes the direction perpendicular to the shear plane (Fig. 5a), y the direction parallel to the shear plane, but perpendicular to the direction of shear (Fig. 5b) and z is the direction of shear.

For high surfactant concentrations ($\rho^s = 0.4$ all three directions behave very similar, i.e. the growth comes to an end after less than 2000 timesteps and the final domain size is between 10 and 15 in lattice units. For $\rho^s = 0.3$, domains grow faster in x-direction, while in the other directions the growth process comes to an end after $t = 2000$ at $L(t) = 15$. For lower surfactant

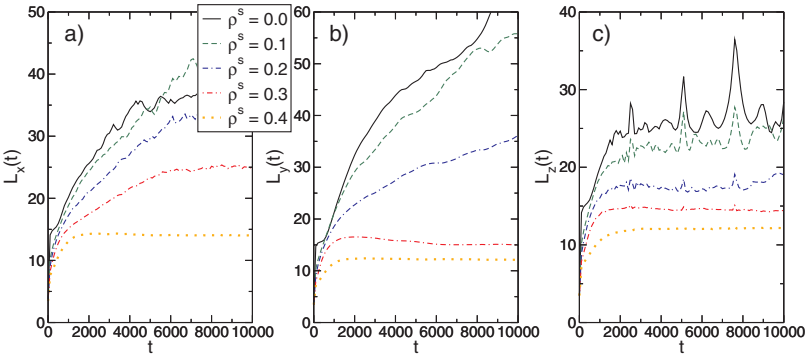

Fig. 5. Domain size $L(\rho^s)$ in x- (**a**), y- (**b**), and z-direction (**c**) for surfactant densities $\rho^s = 0.0,\ 0.1,\ 0.2,\ 0.3,\ 0.4$ and a constant shear rate $\dot{\gamma} = 1.56 \cdot 10^{-3}$

concentrations, the lateral domain size behaves similar in x- and y-directions, except for late times where the growth is limited by the shear. In z-direction, small peaks start to occur for $\rho^s < 0.4$ which increase with decreasing ρ^s. These peaks are due to lamellae forming parallel to the shear and which start to get tilted by the movement of the walls. After a given time, these lamellae are not parallel to the shear anymore and get broken up. Then, the process of lamaellae formation and breaking up starts again.

In Fig. 6 we show an example of the time dependent lateral domain size for a system undergoing oscillatory shear. The shear rate is $\dot{\gamma} = 1.56 \cdot 10^{-3}$, and the frequency of the oscillation is given by $\omega = 0.01$. Here, the upper and lower planes are moved periodically as given by Eq. 6. Here, one can observe a number of new phenomena: For low surfactant concentrations, domain growth is limited in x-direction, but in y direction the domains continue growing until the end of the simulation. This means that we can find tubular structures

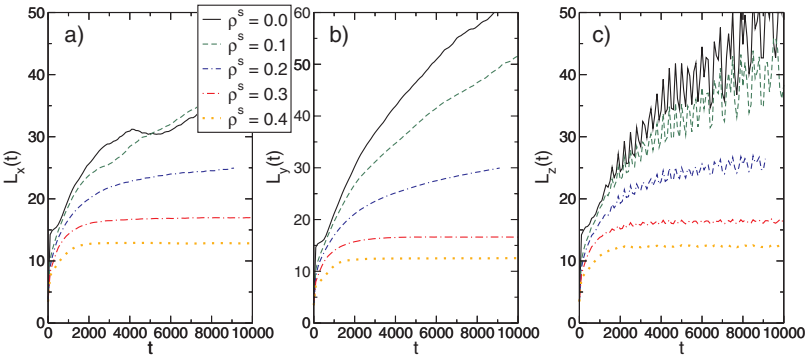

Fig. 6. Domain size $L(\rho^s)$ in x- (**a**), y- (**b**), and z-direction (**c**) for surfactant densities $\rho^s = 0.0,\ 0.1,\ 0.2,\ 0.3,\ 0.4$ and oscillatory shear with $\dot{\gamma} = 1.56 \cdot 10^{-3}$, $\omega = 0.01$

surpassing our system. Also, in z-direction, strong oscillations start to appear due to the continuous growing and destruction of elongated domains.

4 Conclusion

In this report we have presented our first results from ternary amphiphilic lattice-Boltzmann simulations performed on the NEX SX-8 at the HLRS. We have shown that our simulation code performs well on the new machine and that we are able to investigate spinodal decomposition with and without shear. In addition, we have studied the influence of the surfactant concentration on the time dependent lateral domain size.

Acknowledgements

We are grateful for the support of the HPC-Europa programme, funded under the European Commission's Research Infrastructures activity, contract number RII3-CT-2003-506079 and the Höchstleistungsrechenzentrum Stuttgart for providing access to their NEC SX8. We would especially like to thank H. Berger, R. Keller, and P. Lammers for their technical support and J. Chin, and P.V. Coveney for fruitful discussions.

References

1. R. Benzi, S. Succi, and M. Vergassola. The lattice Boltzmann equation: theory and applications. *Phys. Rep.*, 222(3):145–197, 1992.
2. P.L. Bhatnagar, E.P. Gross, and M. Krook. Model for collision processes in gases. I. Small amplitude processes in charged and neutral one-component systems. *Phys. Rev.*, 94(3):511–525, 1954.
3. H. Chen, B.M. Boghosian, P.V. Coveney, and M. Nekovee. A ternary lattice Boltzmann model for amphiphilic fluids. *Proc. R. Soc. Lond. A*, 456:2043–2047, 2000.
4. S. Chen, H. Chen, D. Martínez, and W. Matthaeus. Lattice Boltzmann model for simulation of magnetohydrodynamics. *Phys. Rev. Lett.*, 67(27):3776–3779, 1991.
5. P. Español and P. Warren. Statistical mechanics of dissipative particle dynamics. *Europhys. Lett.*, 30(4):191–196, 1995.
6. T.E. Faber. *Fluid Dynamics for Physicists*. Cambridge University Press, 1995.
7. E.G. Flekkøy, P.V. Coveney, and G.D. Fabritiis. Foundations of dissipative particle dynamics. *Phys. Rev. E*, 62(2):2140–2157, 2000.
8. N. González-Segredo, M. Nekovee, and P.V. Coveney. Three-dimensional lattice-Boltzmann simulations of critical spinodal decomposition in binary immiscible fluids. *Phys. Rev. E*, 67(046304), 2003.
9. J. Harting, M. Harvey, J. Chin, M. Venturoli, and P.V. Coveney. Large-scale lattice Boltzmann simulations of complex fluids: advances through the advent of computational grids. *Phil. Trans. R. Soc. Lond. A*, 363:1895–1915, 2005.

10. J. Harting, M. Venturoli, and P. V. Coveney. Large-scale grid-enabled lattice-Boltzmann simulations of complex fluid flow in porous media and under shear. *Phil. Trans. R. Soc. Lond. A*, 362:1703–1722, 2004.
11. Y. Hashimoto, Y. Chen, and H. Ohashi. Immiscible real-coded lattice gas. *Comp. Phys. Comm.*, 129(1–3):56–62, 2000.
12. 2003. HDF5 – a general purpose library and file format for storing scientific data, http://hdf.ncsa.uiuc.edu/HDF5.
13. P.J. Higuera, S. Succi, and R. Benzi. Lattice gas dynamics with enhanced collisions. *Europhys. Lett.*, 9(4):345–349, 1989.
14. S. Jury, P. Bladon, M. Cates, S. Krishna, M. Hagen, N. Ruddock, and P. Warren. Simulation of amphiphilic mesophases using dissipative particle dynamics. *Phys. Chem. Chem. Phys.*, 1:2051–2056, 1999.
15. A. Lees and S. Edwards. The computer study of transport processes under extreme conditions. *J. Phys. C.*, 5(15):1921–1928, 1972.
16. P.J. Love, M. Nekovee, P.V. Coveney, J. Chin, N. González-Segredo, and J.M.R. Martin. Simulations of amphiphilic fluids using mesoscale lattice-Boltzmann and lattice-gas methods. *Comp. Phys. Comm.*, 153:340–358, 2003.
17. A. Malevanets and R. Kapral. Continuous-velocity lattice-gas model for fluid flow. *Europhys. Lett.*, 44(5):552–558, 1998.
18. M. Nekovee, P.V. Coveney, H. Chen, and B. M. Boghosian. Lattice-Boltzmann model for interacting amphiphilic fluids. *Phys. Rev. E*, 62:8282, 2000.
19. J.-P. Rivet and J. P. Boon. *Lattice Gas Hydrodynamics*. Cambridge University Press, 2001.
20. T. Sakai, Y. Chen, and H. Ohashi. Formation of micelle in the real-coded lattice gas. *Comp. Phys. Comm.*, 129(1–3):75–81, 2000.
21. X. Shan and H. Chen. Lattice Boltzmann model for simulating flows with multiple phases and components. *Phys. Rev. E*, 47(3):1815–1819, 1993.
22. X. Shan and H. Chen. Simulation of nonideal gases and liquid-gas phase transitions by the lattice Boltzmann equation. *Phys. Rev. E*, 49(4):2941–2948, 1994.
23. S. Succi. *The Lattice Boltzmann Equation for Fluid Dynamics and Beyond*. Oxford University Press, 2001.
24. A. Wagner and I. Pagonabarraga. Lees-edwards boundary conditions for lattice Boltzmann. *J. Stat. Phys.*, 107:521, 2002. cond-mat/0103218].
25. A.J. Wagner and J. M. Yeomans. Phase separation under shear in two-dimensional binary fluids. *Phys. Rev. E*, 59(4):4366–4373, 1999.